Preprints of the 21st IFAC World Congress (Virtual)
Berlin, Germany, July 12-17, 2020

Localization from Inertial Data and Sporadic Position Measurements

Antonino Sferlazza * **Luca Zaccarian** ** **Giovanni Garraffa** *
Filippo D'Ippolito *

* *Department of Engineering, University of Palermo, Viale delle Scienze, 90128 Palermo, Italy (e-mail: antonino.sferlazza@unipa.it, giovanni.garraffa01@unipa.it, filippo.dippolito@unipa.it).*
** *CNRS, LAAS, Université de Toulouse, 31400 Toulouse, France, and Dipartimento di Ingegneria Industriale, University of Trento, 38122 Trento, Italy (e-mail: zaccarian@laas.fr).*

Abstract: A novel estimation strategy for inertial navigation in indoor/outdoor environments is proposed with a specific attention to the sporadic nature of the non-periodic measurements. After introducing the inertial navigation model, we introduce an observer providing an asymptotic estimate of the plant state. We use a hybrid dynamical systems representation for our results, in order to provide an effective, and elegant theoretical framework. The estimation error dynamics with the proposed observer shows a peculiar cascaded interconnection of three subsystems (allowing for intuitive gain tuning), with perturbations occurring either on the jump or on the flow dynamics (depending on the specific subsystem under consideration). For this structure, we show global exponential stability of the error dynamics. Hardware-in-the-loop results confirm the effectiveness of the proposed solution.

Keywords: Localization, sampled data observer, sporadic measurements, hybrid systems.

1. INTRODUCTION

Navigation and localization of mobile vehicles represents an important research field witnessing significant efforts in the study of Inertial Navigation Systems (INSs) Hamel and Mahony (2006); Fossen (2011); Zhang et al. (2012). The growing interest in this field mainly arises from the increasing use of autonomous vehicles to accomplish certain tasks that can be dangerous or that require special effort from the human operator. However, autonomous vehicles need precise knowledge of their position and orientation for trajectory tracking or more general navigation and positioning tasks Fossen (1994, 2002); Paull et al. (2014).

Most INSs are based on a 9 degrees of freedom (DOF) Inertial Measurement Unit (IMU). IMUs are indeed typically equipped with three accelerometers for the acceleration measurements in the body frame, three gyros for the measurement of the angular velocity vector, referred to as the Earth Centered Inertial (ECI) frame, three magnetometers allowing for attitude estimation, and a micro-controller in charge of processing the measurement data acquired from the above sensors. A common data fusion process is the strap-down method, consisting in transforming the body frame accelerometer measurements into inertial frame coordinates, by means of the attitude measurements (coming from the estimation of the gravity vector fused with the magnetometers) and then performing an open-loop double integration to estimate the speed and position of the vehicle (Woodman (2007); Zhang et al. (2012); Grip et al. (2013)). It is well known that the strap-down method provides inaccurate estimates, due to the noise and sensor biases combined with the open-loop integration of the acceleration signals. In particular, drifts in the speed and position estimates must be suitably compensated. Consequently, the IMU-based INS works correctly for short time windows, but its behavior degrades rapidly as the integration time increases (Grip et al. (2013)).

In order to cope with this estimation problem, besides the IMU measurements, further position sensors are typically required. In particular, outdoor localization is based on the Global Positioning System (GPS), since it allows for tracking of a mobile object on the Earth, whenever the object can receive the satellite signals. While GPS systems are based on Time-of-Flight (ToF) algorithms, for indoor scenarios different techniques can be used, such as the Received Signal Strength Indicator (RSSI), the Time Difference of Arrival (TDoA) and the ToF distance measurements. Moreover, for indoor scenarios, many communication methods between fixed and mobile devices can be used, like WiFi networks, ultrasonic waves, optical lasers or UltraWideBand radio signals. The recent surveys (Liu et al. (2007); Yassin et al. (2016)) describe different technologies and methods for indoor localization.

In this context, the main challenge is the sensor fusion between the inertial and position measurements coming from various sensors implementing different technologies, operating at different sampling frequencies. Several works have been published to address this challenge. For example (Vik and Fossen (2001)) presents one of the first

⋆ Research supported in part by the Agence Nationale de la Recherche (ANR) via grant Hybrid And Networked Dynamical sYstems (HANDY), number ANR-18-CE40-0010.

nonlinear observers for GPS and IMU sensor data fusion. In (Zhao and Slotine (2005)), based on contraction theory, a deterministic nonlinear observer is proposed, which takes into account the sampled-data and sporadic nature of the measurements, but using additional velocity measurements (not used in this paper). When these velocity measurements are available, a nonlinear observer for inertial navigation is proposed in Grip et al. (2013), which uses a quaternion-based attitude representation. That work was then extended in Bryne et al. (2014) by introducing time-varying observer gains. Similar results relying on velocity measurements are given in Fusini et al. (2014), which addresses nonlinear position, velocity and attitude estimation for Unmanned Aerial Vehicles (UAVs).

In this paper we propose a novel estimation strategy for inertial navigation in indoor/outdoor environments, with specific attention to the sporadic nature of position-only measurements (namely we do not assume the presence of any velocity sensors). The motivation for our work is that, especially when operating with beacons and non-periodic or unreliable communication channels, it is well known that the sampled position measurements are far from being available at a fixed frequency. To rigorously represent this scenario, we adopt the hybrid dynamical systems modeling framework of Goebel et al. (2012), which provides an effective and elegant notation, in addition to a number of useful well-posedness results. This hybrid framework has been already used in other works dealing with the design of observers with sporadic measurements Ferrante et al. (2016); Li et al. (2018); Sferlazza et al. (2019); Ferrante et al. (2019), due to its suitability for obtaining accurate models of systems with sampled measurements and non-periodic time-of-arrival. While those approaches can solve the estimation problem addressed here, the explicit solution that we build in this paper is more effective in terms of the tunability of the estimation error dynamics due to its peculiar cascaded structure.

The structure of this paper is as follows. After introducing the inertial navigation model in Section 2, we illustrate the dynamics of the proposed observer in Section 3, first discussing the implementation and then deriving the error dynamics and their cascaded structure. Finally, in Section 4, we present some experiments carried out using a hardware-in-the-loop method. The experiments confirm the effectiveness of the proposed solution in providing accurate estimates also in the presence of measurement noise.

Notation: $\mathbb{R}^n$ denotes the n-dimensional Euclidean space. $\mathbb{R}_{\geq 0}$ denotes the set of nonnegative real numbers. $\mathbb{Z}$ denotes the set of all integers, while $\mathbb{Z}_{\geq 0}$ denotes the set of nonnegative integers. $\mathbb{B}$ denotes the closed unit ball, of appropriate dimensions, in the Euclidean norm. I_q denotes the identity matrix of dimension $q \in \mathbb{Z}_{\geq 0}$. $\lambda_m(S)$ and $\lambda_M(S)$ denote, respectively, the minimum and the maximum eigenvalues of a symmetric matrix S. x^+ denotes the state of a hybrid system after a jump. $|x|$ denotes the Euclidean norm of a vector $x \in \mathbb{R}^n$. B, and N denote the BODY and NED (North-East-Down) reference frames, respectively.

2. SPORADIC POSITION MEASUREMENTS IN AN INERTIAL NAVIGATION SYSTEM

Consider the strap-down model of an Inertial Navigation System (INS) given by: (Bryne et al., 2014, Eq.s (2)-(3)):

$$\dot{\boldsymbol{v}}^n = \boldsymbol{V}(\boldsymbol{\xi}_b^n)\boldsymbol{\gamma}^b + \boldsymbol{g}, \tag{1}$$
$$\dot{\boldsymbol{p}}^n = \boldsymbol{v}^n. \tag{2}$$

where $\boldsymbol{p}^n := [p_x \ p_y \ p_z]^\top$ and $\boldsymbol{v}^n := [v_x \ v_y \ v_z]^\top$ are respectively the position and velocity vectors expressed in N coordinates $(x,\ y,\ z)$, $\boldsymbol{g} := [0 \ 0 \ g]^\top$ is the gravity acceleration referred to the N-frame, $\boldsymbol{\gamma}^b := [\gamma_x \gamma_y \gamma_z]^\top$ is the acceleration measurement provided by the IMU expressed in the B-frame, $\boldsymbol{\xi}_b^n := [\xi_0 \ \xi_1 \ \xi_2 \ \xi_3]^\top$ is the quaternion vector, describing the orientation of the B-frame relative to the N-frame, and matrix $\boldsymbol{V}(\boldsymbol{\xi}_b^n)$ is the rotation matrix from the B-frame to the N-frame, as a function of the associated quaternion, corresponding to

$$\boldsymbol{V}(\boldsymbol{\xi}_b^n) := \begin{bmatrix} \xi_0^2+\xi_1^2-\xi_2^2-\xi_3^2 & 2(\xi_1\xi_2-\xi_0\xi_3) & 2(\xi_1\xi_3+\xi_0\xi_2) \\ 2(\xi_1\xi_2+\xi_0\xi_3) & \xi_0^2-\xi_1^2+\xi_2^2-\xi_3^2 & 2(\xi_2\xi_3-\xi_0\xi_1) \\ 2(\xi_1\xi_3-\xi_0\xi_2) & 2(\xi_2\xi_3+\xi_0\xi_1) & \xi_0^2-\xi_1^2-\xi_2^2+\xi_3^2 \end{bmatrix}.$$

The inertial model (1), (2) is obtained under the assumption that the Earth angular velocity about the z-axis of the Earth-Centered Inertial (ECI) frame is small, so that it can be neglected (Grip et al., 2013, Remark 2). For further details about (1), (2) the reader is referred to (Alonge et al., 2019, Section II).

The strap-down inertial navigation algorithm (Zhao and Slotine (2005); Grip et al. (2013)) is not robust, because the speed and the position vectors are obtained by open-loop integration of the acceleration and this leads to drift problems. To solve these observability problems, a position measurement is used, provided by a Global Positioning System (GPS), for outdoor navigation, or beacons, for indoor navigation. Consequently, problems arise because these position measurements are available with a significantly lower sampling rate, as compared to the IMU signals. Moreover the time between two consecutive position measurements is not constant, thus providing a so-called sporadic position measurements situation Ferrante et al. (2016, 2019). In order to formalize the above described setting, we assume in this paper that no velocity measurement is available and that the only output of system (1)-(2) is represented by the vector $\boldsymbol{y} = \boldsymbol{p}^n$, only accessible at discrete instants of time, resulting in a sequence of 3-dimensional vectors $\boldsymbol{y}_k$, $k \in \mathbb{Z}_{\geq 1}$, defined as:

$$\boldsymbol{y}_k = \boldsymbol{p}_k^n := \boldsymbol{p}^n(t_k), \tag{3}$$

where t_k, $k \in \mathbb{Z}_{\geq 1}$, is a sequence of increasing non-negative real numbers that satisfies the following assumption:

Assumption 1. There exist scalars T_m and T_M, with $0 < T_m \leq T_M$, such that:

$$T_m \leq |t_{k+1} - t_k| \leq T_M, \quad \forall\, k \in \mathbb{Z}_{\geq 1}. \tag{4}$$

Assumption 1 essentially requires that the sporadic measurements $\boldsymbol{y}_k$ be available with intersample times that are lower and upper bounded by positive constants $T_m \leq T_M$ whose knowledge is not required by the estimation algorithm proposed here. As a consequence, Assumption 1 appears to be an extremely mild assumption ruling out the defective cases of Zeno behaviors (because T_m is greater

than zero) and the situation of sporadic measurements whose occurrence becomes increasingly rare as time grows.

Using the hybrid systems formalism of Goebel et al. (2012), it is possible to represent the sampled-data system associated with setting (1)–(3) as follows:

$$\begin{cases} \dot{\boldsymbol{v}}^n = \boldsymbol{V}(\boldsymbol{\xi}_b^n)\boldsymbol{\gamma}^b + \boldsymbol{g}, \\ \dot{\boldsymbol{p}}^n = \boldsymbol{v}^n, \\ \dot{\tau} = 1, \end{cases} \qquad (\boldsymbol{v}^n, \boldsymbol{p}^n, \tau) \in \mathcal{C}, \tag{5a}$$

$$\begin{cases} \boldsymbol{v}^{n+} = \boldsymbol{v}^n, \\ \boldsymbol{p}^{n+} = \boldsymbol{p}^n, \\ \tau^+ = 0, \end{cases} \qquad (\boldsymbol{v}^n, \boldsymbol{p}^n, \tau) \in \mathcal{D}, \tag{5b}$$

$$\boldsymbol{y} = \boldsymbol{p}^n, \tag{5c}$$

where the timer τ is an additional state variable keeping track of the elapsed time since the last measurement, while sets $\mathcal{C}$ and $\mathcal{D}$ are respectively the so-called *flow set* and *jump set*, defined as:

$$\mathcal{C} := \mathbb{R}^3 \times \mathbb{R}^3 \times [0, T_M], \tag{6}$$

$$\mathcal{D} := \mathbb{R}^3 \times \mathbb{R}^3 \times [T_m, T_M]. \tag{7}$$

The impulsive nature of the available measurement is represented by the extra property that $\boldsymbol{y} = \boldsymbol{p}^n$ is only available at the jump times.

3. CONTINUOUS-DISCRETE OBSERVER ARCHITECTURE

3.1 Observer dynamics

In this paper, we propose an observer whose structure implicitly complies with the restriction specified in Assumption 1 about the available measurements. Our observer is capable of providing an asymptotic estimate of the plant state, for any sequence of sampling times t_k at which the sampled output is available, as long as these times satisfy Assumption 1 for some (not known) values of $0 < T_m \leq T_M$.

The hybrid structure of the proposed observer is the following one

$$\begin{cases} \dot{\hat{\boldsymbol{v}}}^n = \boldsymbol{V}(\boldsymbol{\xi}_b^n)\boldsymbol{\gamma}^b + \boldsymbol{g}, \\ \dot{\hat{\boldsymbol{p}}}^n = \hat{\boldsymbol{v}}^n, \\ \dot{\tau} = 1, \\ \dot{\tilde{\boldsymbol{p}}} = 0, \end{cases} \qquad (\hat{\boldsymbol{v}}^n, \hat{\boldsymbol{p}}^n, \tau, \tilde{\boldsymbol{p}}) \in \mathcal{C} \times \mathbb{R}^3, \tag{8a}$$

$$\begin{cases} \hat{\boldsymbol{v}}^{n+} = \hat{\boldsymbol{v}}^n + (1-\alpha_v)\left(\dfrac{\boldsymbol{p}^n - \hat{\boldsymbol{p}}^n - \tilde{\boldsymbol{p}}}{\tau}\right), \\ \hat{\boldsymbol{p}}^{n+} = \hat{\boldsymbol{p}}^n + (1-\alpha_p)(\boldsymbol{p}^n - \hat{\boldsymbol{p}}^n), \\ \tau^+ = 0, \\ \tilde{\boldsymbol{p}}^+ = \alpha_p(\boldsymbol{p}^n - \hat{\boldsymbol{p}}^n) \end{cases} \qquad (\hat{\boldsymbol{v}}^n, \hat{\boldsymbol{p}}^n, \tau, \tilde{\boldsymbol{p}}) \in \mathcal{D} \times \mathbb{R}^3, \tag{8b}$$

where $\tilde{\boldsymbol{p}}$ is an auxiliary "zero-order hold" state vector propagating the last position correction term across the intersample interval, and α_v and α_p are two positive gains that may be tuned to suitably adjust the estimation error transient. Note that the measurement $\boldsymbol{y} = \boldsymbol{p}^n$ is only used in the jump dynamics of our observer, which is then compliant with the measurement constraints imposed by Assumption 1.

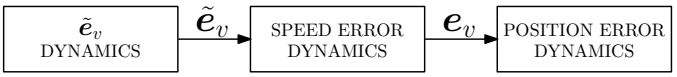

Fig. 1. Block diagram of the speed and position error dynamics.

As compared to the architecture used in Alonge et al. (2019), observer (8) considers a different jump map with an extra auxiliary state vector $\tilde{\boldsymbol{p}}$. This is necessary because Alonge et al. (2019) addresses a simpler problem where both the position and the speed are simultaneously measured. In the setting addressed here, where only the sampled position measurement is available, a more sophisticated dynamic correction is required.

3.2 Error Dynamics and Main Result

The main result of this work proves stability and convergence of the estimation error in the extended error space corresponding to the error variables

$$\boldsymbol{e} := \begin{bmatrix} \boldsymbol{e}_v \\ \boldsymbol{e}_p \end{bmatrix} := \begin{bmatrix} \boldsymbol{v}^n \\ \boldsymbol{p}^n \end{bmatrix} - \begin{bmatrix} \hat{\boldsymbol{v}}^n \\ \hat{\boldsymbol{p}}^n \end{bmatrix} \tag{9a}$$

$$\tilde{\boldsymbol{e}}_v := \boldsymbol{e}_p - \tilde{\boldsymbol{p}} - \tau \boldsymbol{e}_v \tag{9b}$$

and provides design rules to select the tuning gains α_v and α_p in (8). In particular, with the error variables (9), the corresponding error dynamics issued from (5)-(8) is well represented by the cascaded structure schematically shown in Figure 1. In this figure, the upper subsystem, governed by the dynamics of $\tilde{\boldsymbol{e}}_v$, converges to zero in finite time at the first measurement instant; the middle subsystem, governed by the velocity error dynamics $\boldsymbol{e}_v$, provides a constant continuous-time behavior in the inter-measurement periods and a discretely converging dynamics (tunable by adjusting α_v) at the measurement instants, perturbed by input $\tilde{\boldsymbol{e}}_v$. Finally, the third subsystem, governed by the position error dynamics $\boldsymbol{e}_p$, provides a constant continuous-time behavior perturbed by the velocity error $\boldsymbol{e}_v$ in the inter-measurement periods, and a discretely converging dynamics (tunable by adjusting α_p) at the measurement instants.

For clarity of exposition, we write the three dynamics represented in Figure 1 as three different systems, even though it is emphasized that the variable τ governing the jumps is the same one for all of them. By considering (5) and (8), the hybrid position error dynamics can be written as:

$$\begin{cases} \dot{\boldsymbol{e}}_p = \boldsymbol{e}_v, \\ \dot{\tau} = 1, \end{cases} \qquad (\boldsymbol{e}_p, \tau) \in \mathbb{R}^3 \times [0, T_M], \tag{10a}$$

$$\begin{cases} \boldsymbol{e}_p{}^+ = \alpha_p \boldsymbol{e}_p, \\ \tau^+ = 0, \end{cases} \qquad (\boldsymbol{e}_p, \tau) \in \mathbb{R}^3 \times [T_m, T_M], \tag{10b}$$

while, the speed error dynamics can be written as:

$$\begin{cases} \dot{\boldsymbol{e}}_v = 0, \\ \dot{\tau} = 1, \end{cases} \qquad (\boldsymbol{e}_v, \tau) \in \mathbb{R}^3 \times [0, T_M], \tag{11a}$$

$$\begin{cases} \boldsymbol{e}_v{}^+ = \alpha_v \boldsymbol{e}_v + \dfrac{\alpha_v - 1}{\tau}\tilde{\boldsymbol{e}}_v, \\ \tau^+ = 0, \end{cases} \qquad (\boldsymbol{e}_v, \tau) \in \mathbb{R}^3 \times [T_m, T_M]. \tag{11b}$$

Finally, the dynamics of $\tilde{\boldsymbol{e}}_v$ is governed by

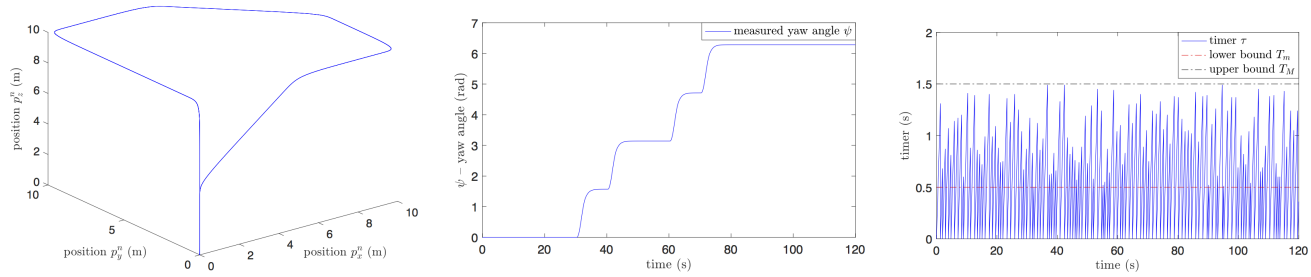

(a) (b) (c)

Fig. 2. Reference position trajectory (a). Reference yaw angle (b). Evolution of the timer variable τ showing the sporadic nature of the sampled position measurements (c).

$$\begin{cases} \dot{\tilde{\boldsymbol{e}}}_v = 0, \\ \dot{\tau} = 1, \end{cases} \qquad (\tilde{\boldsymbol{e}}_v, \tau) \in \mathbb{R}^3 \times [0, T_M], \tag{12a}$$

$$\begin{cases} \tilde{\boldsymbol{e}}_v^{\,+} = 0, \\ \tau^+ = 0, \end{cases} \qquad (\tilde{\boldsymbol{e}}_v, \tau) \in \mathbb{R}^3 \times [T_m, T_M]. \tag{12b}$$

Remark 1. The cascaded interconnection represented in Figure 1 and whose dynamics correspond to (10), (11) and (12) is somewhat peculiar because: 1) the upper subsystem converges to zero in finite time (at the first jump); 2) the middle subsystem converges asymptotically to zero being perturbed by the upper subsystem across jumps; 3) the lower subsystem converges asymptotically to zero being perturbed by the upper subsystem along flows. This somewhat peculiar continuous-discrete cascaded interconnection naturally emerges from the continuous-discrete nature of the observer. ⌟

Our main result provides necessary and sufficient conditions for the gains α_p and α_v in the observer dynamics (8) to ensure global exponential stability (GES) of the compact set (the attractor):

$$\mathcal{A} := \Big\{ (\boldsymbol{e}, \tilde{\boldsymbol{e}}_v, \tau) : \boldsymbol{e} = 0, \tilde{\boldsymbol{e}}_v = 0, \tau \in [0, T_M] \Big\}, \tag{13}$$

for the error dynamics (10), (11) and (12). The attractor in (13) corresponds to the set where the estimation error is zero, therefore our main result establishes necessary and sufficient conditions for exponential estimation of the unmeasured states $\boldsymbol{p}^n$ and $\boldsymbol{v}^n$.

Theorem 1. Set $\mathcal{A}$ in (13) is globally exponentially stable for the error dynamics (10), (11) and (12) if and only if the gains α_p and α_v satisfy $|\alpha_p| < 1$ and $|\alpha_v| < 1$. In particular, those conditions hold if and only if there exist positive scalars κ and λ such that all solutions to (5)–(8) satisfy

$$\begin{bmatrix} \boldsymbol{v}^n(t,j) - \hat{\boldsymbol{v}}^n(t,j) \\ \boldsymbol{p}^n(t,j) - \hat{\boldsymbol{p}}^n(t,j) \end{bmatrix} = \begin{bmatrix} \boldsymbol{e}_v(t,j) \\ \boldsymbol{e}_p(t,j) \end{bmatrix} \leq \kappa \mathrm{e}^{-\lambda(t+j)} \left| \begin{bmatrix} \boldsymbol{e}_v(0,0) \\ \boldsymbol{e}_p(0,0) \\ \tilde{\boldsymbol{e}}_v(0,0) \end{bmatrix} \right|. \tag{14}$$

While the proof of Theorem 1 is omitted for lack of space, we emphasize here that the error dynamics (10), (11) and (12) satisfies the hybrid basic assumptions of (Goebel et al., 2012, As. 6.5) (which in this single-valued case corresponds to checking that the flow and jump sets are closed and the flow and jump maps are continuous in these respective sets). Therefore, since the attractor $\mathcal{A}$ in (13) is compact, according to (Goebel et al., 2012, Ch. 7), the established GAS property is uniform, namely the proposed observer (8) provides uniformly convergent asymptotic estimates of $\boldsymbol{p}^n$ and $\boldsymbol{v}^n$ under the stated assumptions on the gains. Finally, due to (Goebel et al., 2012, Ch. 7), sufficiently small modeling and measurement errors do not destroy such a stability property, but provide a graceful performance degradation in a semiglobal practical sense.

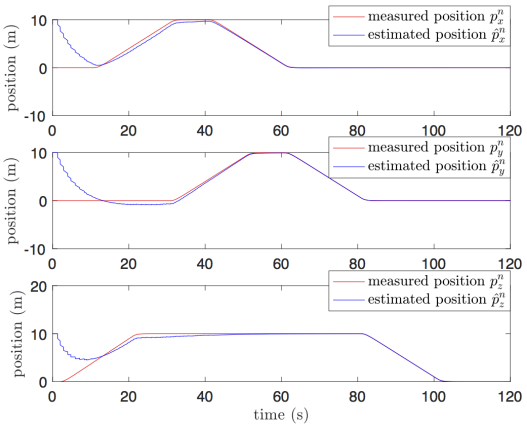

Fig. 3. Actual and estimated positions in *test 1* (noise-free).

4. HARDWARE-IN-THE-LOOP RESULTS

We test observer (8) by running some hardware-in-the-loop experiments. To this end, the hybrid dynamics (8) has been implemented in a Raspberry-PI 3 with a sampling frequency of 100 Hz. While, by means of Matlab®-simulink®, a suitable realistic scenario has been simulated resembling a possible path associated to the motion of a mobile vehicle. The corresponding trajectory is shown in Figures 2(a) and 2(b), which display the reference position and yaw angle, respectively. In the hardware-in-the-loop setup, sampled measurements of this trajectory, as well as accelerations and attitude angles are sent to the Raspberry. In particular, the IMU data corresponding to the accelerations and attitude angles are provided to the Raspberry periodically with a fixed frequency coinciding with its operating frequency (100 Hz), while the sporadic position measurements are available at random instants of time satisfying Assumption 1 for some small enough T_m and some large enough T_M. Even though these values are not important (the observer dynamics is independent of them), here we selected $T_m = 0.5$s and $T_M = 1.5$s. The evolution of the timer variable τ is reported in Fig. 2(c), showing that the measurements occur randomly in the interval $[T_m,\ T_M]$, according to the described dynamics.

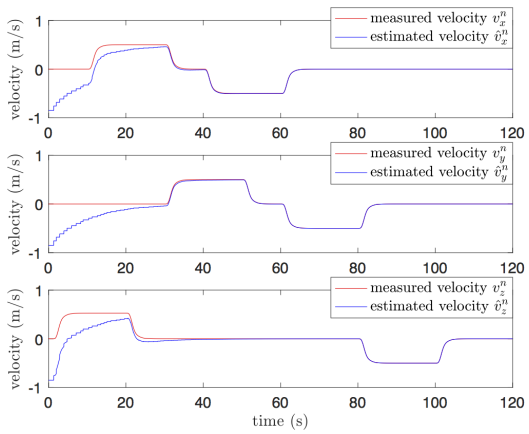

Fig. 4. Actual and estimated velocities in *test 1* (noise-free).

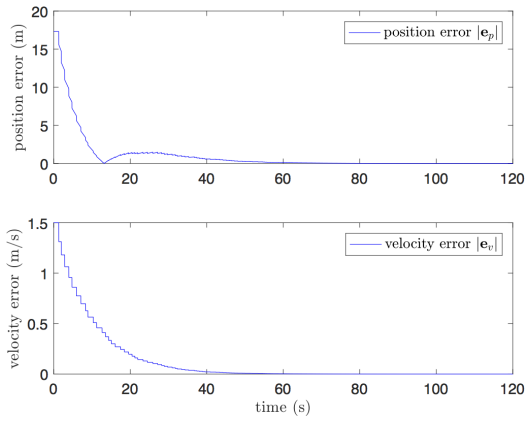

Fig. 5. Position errors $\boldsymbol{e}_p$ (upper plot) and velocity errors $\boldsymbol{e}_p$ (bottom plot) in *test 1* (noise-free).

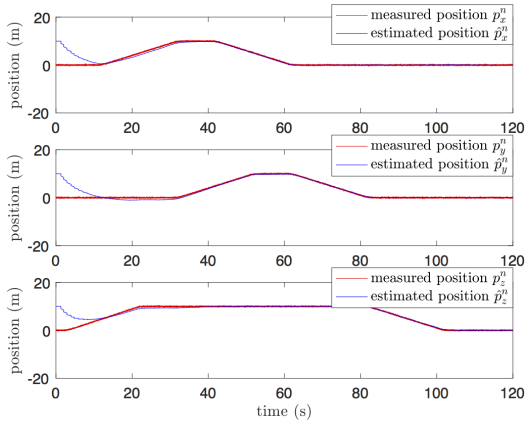

Fig. 6. Actual and estimated positions in *test 2* (noisy).

The parameters of the observer have been fixed at $\alpha_v = 0.9$ and $\alpha_p = 0.9$ and the initial conditions are $\boldsymbol{p}_0^n = [10\ 10\ 10]$ and $\boldsymbol{v}_0^n = [-0.85\ \ -0.85\ \ -0.85]$. Two tests have been performed: in *test 1* (noise-free case) the position trajectory of Fig. 2(a) has been exactly sampled, at the sporadic times discussed above, and fed to the observer. Similarly, the accelerations $\boldsymbol{\gamma}^b$ and the attitude angles $\boldsymbol{\xi}_b^n$ have been fed to the observer in a noise-free scenario. In *test 2* (noisy case) for the same values of the observer parameters and initial conditions, the measurements have been corrupted by noise. In particular, the accelerations

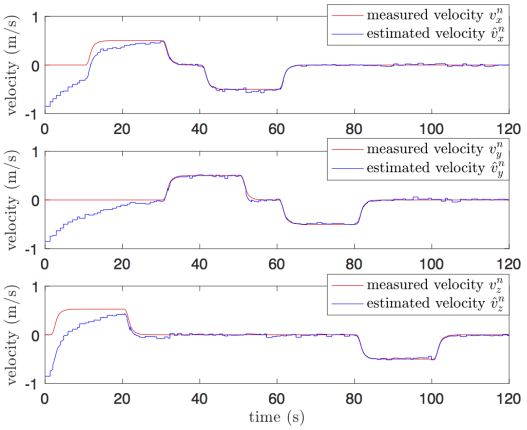

Fig. 7. Actual and estimated velocities in *test 2* (noisy).

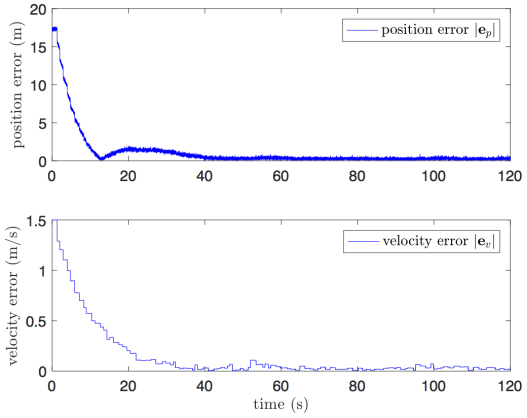

Fig. 8. Position errors $\boldsymbol{e}_p$ (upper plot) and velocity errors $\boldsymbol{e}_p$ (bottom plot) in *test 2* (noisy).

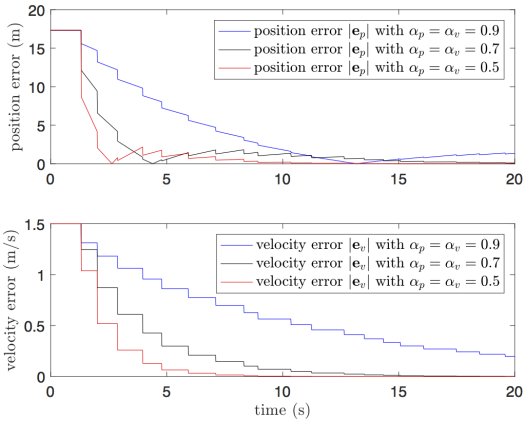

Fig. 9. Waveforms of the position error $\boldsymbol{e}_p$ (upper plot) and of the velocity error $\boldsymbol{e}_p$ (bottom plot) for different values of α_p and α_v.

have been corrupted by a Gaussian zero mean white noise having standard deviation equal to 0.04 m/s^2, while the position has been corrupted by a Gaussian zero mean white noise having standard deviation equal to 0.5 m.

The results of the noise-free *test 1* are shown in Figures 3-5. In particular Figures 3 and 4 show the real and the estimated positions and velocities. It is apparent that the estimated variables exponentially converge to the corresponding state variables (all the errors exponentially converge to zero). The hybrid behavior of the estimate

is clearly visible, especially during the initial transient. Indeed, in Fig. 5 the velocity error is constant during flowing, and decreases across jumps, as expected from the theoretical results Theorem 1, while the position error respects the bound given in Theorem 1. Figure 5 provides further insight by showing suitably zoomed (transient and steady-state) areas from Figure 5.

Similar tests have been provided for *test 2* (noisy case), and are reported in Figures 6-8. These noisy tests confirm that the observer is able to cope with noisy measurements, since both the position and the velocity are well estimated by a suitable filtering action of the measurement noise.

Finally Figure 9 shows the position error $\boldsymbol{e}_p$ and the velocity error $\boldsymbol{e}_v$ for different values of α_p and α_v. As one may expect from the error dynamics characterized in Theorem 1, the closer α_p and α_v are to zero, the higher the convergence rate of the estimation error will be, but a higher convergence rate leads to a reduced filtering action on the measurement noise. The choice of α_p and α_v then should be carried out as a trade-off between these two goals. Note also that the convergence rate is influenced by the values of T_m and T_M. Indeed, if the measurements are accessible less frequently, then the convergence rate results to be slower.

5. CONCLUSIONS

In this paper, a novel estimation strategy for inertial navigation in indoor/outdoor environments has been proposed with specific attention to the sporadic nature of the sampled-data measurements. After introducing the inertial navigation model, an observer providing exponentially converging position and velocity estimates has been proposed. A hybrid dynamical systems framework has been used for presenting our results. The main theorem proves uniform exponential convergence to zero of the estimation error, together with an intuitive selection of the observer gains. Hardware-in-the-loop experiments confirmed the effectiveness of the proposed approach and the capability of the described observer to also deal with measurement noise.

REFERENCES

Alonge, F., D'Ippolito, F., Garraffa, G., and Sferlazza, A. (2019). A hybrid observer for localization of mobile vehicles with asynchronous measurements. *Asian Journal of Control*, 21, 1506–1521.

Bryne, T.H., Fossen, T., and Johansen, T.A. (2014). Nonlinear observer with time-varying gains for inertial navigation aided by satellite reference systems in dynamic positioning. In *IEEE Mediterranean Conference on Control and Automation*, 1353–1360. IEEE, Palermo, Italy.

Ferrante, F., Gouaisbaut, F., Sanfelice, R.G., and Tarbouriech, S. (2016). State estimation of linear systems in the presence of sporadic measurements. *Automatica*, 73, 101–109.

Ferrante, F., Gouaisbaut, F., Sanfelice, R.G., and Tarbouriech, S. (2019). $\mathcal{L}_2$ state estimation with guaranteed convergence speed in the presence of sporadic measurements. *IEEE Transactions on Automatic Control*, 64(8), 3362–3369.

Fossen, T.I. (1994). *Guidance and control of ocean vehicles*. John Wiley & Sons.

Fossen, T.I. (2002). *Marine Control Systems: Guidance, Navigation and Control of Ships, Rigs and Underwater Vehicles*. Marine Cybernetics, Trondheim, Norway.

Fossen, T.I. (2011). *Handbook of marine craft hydrodynamics and motion control*. John Wiley & Sons.

Fusini, L., Fossen, T., and Johansen, T.A. (2014). A uniformly semiglobally exponentially stable nonlinear observer for GNSS-and camera-aided inertial navigation. In *IEEE Mediterranean Conference on Control and Automation*, 1031–1036. IEEE, Palermo, Italy.

Goebel, R., Sanfelice, R.G., and Teel, A.R. (2012). *Hybrid Dynamical Systems: modeling, stability, and robustness*. Princeton University Press.

Grip, H.F., Fossen, T., Johansen, T.A., and Saberi, A. (2013). Nonlinear observer for GNSS-aided inertial navigation with quaternion-based attitude estimation. In *IEEE American Control Conference*, 272–279. IEEE, Washington DC, United States.

Hamel, T. and Mahony, R. (2006). Attitude estimation on SO(3) based on direct inertial measurements. In *IEEE International Conference on Robotics and Automation*, 2170–2175. IEEE, Orlando, United States.

Li, Y., Phillips, S., and Sanfelice, R.G. (2018). Robust distributed estimation for linear systems under intermittent information. *IEEE Transactions on Automatic Control*, 63(4), 973–988.

Liu, H., Darabi, H., Banerjee, P., and Liu, J. (2007). Survey of wireless indoor positioning techniques and systems. *IEEE Transactions on Systems, Man, and Cybernetics, Part C (Applications and Reviews)*, 37(6), 1067–1080.

Paull, L., Saeedi, S., Seto, M., and Li, H. (2014). AUV navigation and localization: A review. *Oceanic Engineering, IEEE Journal of*, 39(1), 131–149.

Sferlazza, A., Tarbouriech, S., and Zaccarian, L. (2019). Time-varying sampled-data observer with asynchronous measurements. *IEEE Transactions on Automatic Control*, 64(2), 869–876.

Vik, B. and Fossen, T. (2001). A nonlinear observer for GPS and INS integration. In *IEEE Conference on Decision and Control*, volume 3, 2956–2961. IEEE, Orlando, United States.

Woodman, O.J. (2007). An introduction to inertial navigation. Technical report, University of Cambridge, Computer Laboratory.

Yassin, A., Nasser, Y., Awad, M., Al-Dubai, A., Liu, R., Yuen, C., Raulefs, R., and Aboutanios, E. (2016). Recent advances in indoor localization: A survey on theoretical approaches and applications. *IEEE Communications Surveys & Tutorials*, 19(2), 1327–1346.

Zhang, W., Ghogho, M., and Yuan, B. (2012). Mathematical model and matlab simulation of strapdown inertial navigation system. *Modelling and Simulation in Engineering*, 2012, 1–25.

Zhao, Y. and Slotine, J.J.E. (2005). Discrete nonlinear observers for inertial navigation. *Systems & control letters*, 54(9), 887–898.